

# Modified Titanate Nanotubes for the Production of Novel Aliphatic Polyurethane Nanocomposites

Wesley F. Monteiro,<sup>1</sup> Cláudia A.B. dos Santos,<sup>1</sup> Mauricio S. Hoffmann,<sup>1</sup> Carlos L.P. Carone,<sup>1</sup> Sandra M.O. Einloft,<sup>1,2</sup> Michèle O. de Souza,<sup>3\*</sup> Rosane A. Ligabue<sup>1,2\*</sup>

<sup>1</sup>Post-Graduation Program in Materials Engineering and Technology, PUCRS, Porto Alegre, 90619900, Brazil

<sup>2</sup>School of Chemistry, PUCRS, Porto Alegre, 90619900, Brazil

<sup>3</sup>Institute of Chemistry, UFRGS, Porto Alegre, 90650-001, Brazil

**Aliphatic polyurethane (PU) nanocomposites were prepared using modified titanate nanotubes (TNTs) as filler in order to improve the mechanical and thermal properties of the initial polymer. With a view to achieving greater interaction between the polymer chains and TNTs, the latter was functionalized with hexamethylene diisocyanate (H) and/or aminopropyl trimethoxysilane groups (A), producing the modified nanotubes TNTH, TNTA, or TNTHA. The thermogravimetric analyses used to quantify the amount of anchored diisocyanate or/and silanol groups in the nanotubes identified the H function as the best functional group in terms of improving the filler-PU compatibility. Transmission electron microscopy, field emission scanning electron microscopy, and atomic force microscopy analyses of the PU nanocomposites containing the three different fillers showed good TNT dispersion. The TNTHA nanotubes functionalized with both groups through the reaction between the H function already anchored on the TNTs and the A group, forming a monourea anchored group, significantly improved the mechanical and thermal properties of PU nanocomposites. POLYM. COMPOS., 40:2292-2300, 2019. © 2018 Society of Plastics Engineers**

## INTRODUCTION

The synthesis of polymeric nanocomposites has attracted substantial scientific and industrial interest for their ability to modify and/or improve the thermal, mechanical, optical, and barrier properties of several traditional polymers [1–3]. In this context, polyurethane (PU) is a polymer with a wide variety of applications, since it can be

easily molded, injected, extruded, and recycled [4]. Moreover, PU matrices have proved to be suitable for the addition of different fillers, such as clays [5], zinc oxide [6], silica [7], titanium dioxide [8], and synthetic talc [9, 10], among others. Corresponding studies on these PU nanocomposites showed an improvement in their mechanical properties, thermal stability, and hydrophobic behavior. The use of fillers with a high specific surface area has been related to increased polymer crystallinity and thermal stability. These property modifications have been attributed to fillers, which act as nucleating agents.

Multilayer carbon nanotubes [11], halloysite clay [12], and hybrids of these materials [13], which have a high specific surface area and tubular morphology, were also used to produce polymeric nanocomposites with significantly improved tensile strength, Young's modulus, and elongation at break. In this respect, titanate nanotubes (TNTs) emerge as a promising alternative filler due to their low-cost and easy synthesis. TNTs can be obtained via a simple hydrothermal method first described by Kasuga et al. [14]. TNTs are used in several different applications, including uranium and palladium adsorption [15, 16], CO<sub>2</sub> capture [17], and as catalysts [18–20], due to their uniform tubular morphology and high specific surface area ( $\approx 170$  m<sup>2</sup>/g), making them suitable for tube surface modification and low toxicity [21]. However, a drawback of TNTs is their hydrophilic nature, caused by the presence of high concentrations of hydroxyl groups at the nanotube surface, making it difficult for TNT to disperse into the polymeric matrices and thereby forming filler clusters [22]. One way of mitigating this problem is by modifying the nanotubes through surface functionalization. For example, the presence of organosilanol groups such as 3-aminopropyl triethoxysilane [23], allyltriethoxysilane and *n*-propyltriethoxysilane [24] at the nanotube surface enhances filler dispersion due to favorable chemical interactions between the polymer chain and functionalized material [25, 26].

Correspondence to: M.O. de Souza; e-mail: rligabue@pucrs.br and R.A. Ligabue; e-mail: michele.souza@ufrgs.br

Contract grant sponsor: CNPq (National Council for Scientific and Technological Development). contract grant sponsor: CAPES (Coordination for the Improvement of Higher Education Personnel).

DOI 10.1002/pc.25038

Published online in Wiley Online Library (wileyonlinelibrary.com).

© 2018 Society of Plastics Engineers

TNT-based hybrid nanostructures allow good compatibility with organic matrices. Although PU-based nanocomposites have been widely investigated, to the best of our knowledge, there are few studies on the use of functionalized TNTs as filler for these polymers, particularly its use *in situ* to obtain PU nanocomposites. As such, this study aims to synthesize and characterize PU nanocomposites using TNTs modified with hexamethylene diisocyanate (H) and/or aminopropyl trimethoxysilane (A). The effect of the functionalized TNTs on the thermal, mechanical, and morphological properties of the synthesized nanocomposites is also evaluated.

## EXPERIMENTAL

### Materials

Polycaprolactone diol (PCL, MM = 2,000 g mol<sup>-1</sup>, Sigma-Aldrich) was dried before use. Hexamethylene diisocyanate (HDI, Merck), dibutyltin dilaurate (DBTDL, Miracema-Nuodex Ind.), methyl ethyl ketone (MEK, Merck), aminopropyl trimethoxysilane (APTMS, 97%, Sigma-Aldrich), titanium dioxide (TiO<sub>2</sub>, 98% anatase phase, JB Química), and sodium hydroxide (NaOH, 99%, Vetec) were used as received.

### TNT Synthesis

TNTs were synthesized using the hydrothermal method adapted from the literature [14]. Initially, 1.5 g of TiO<sub>2</sub> was added to 120 mL of 10 M NaOH solution under magnetic stirring, at room temperature, for 30 min. Next, the solution was transferred to a Teflon-coated stainless steel reactor (200 cm<sup>3</sup>) and the system was maintained at 130–140°C for 72 h. The resulting precipitate was centrifuged and washed with distilled water until a pH 8. The TNTs were dried at 80°C for 6 h and kept in a desiccator.

### Functionalization of the TNTs

We added 1 g of TNT (previously dried), the functionalizing agent (molar ratio TNT:agent = 1:1) and 20 mL of MEK to a Schlenk flask. The reaction system was kept under reflux (40°C), an inert atmosphere (N<sub>2</sub>), and magnetic stirring for 2.5 h. The solvent was then removed under reduced pressure and the solid product was dried at 45°C for 2 h. This method produced three different modified TNTs, namely TNTH, TNTA, and TNTHA, corresponding respectively to TNTs containing H, A, and the product of the reaction between both (HA). In the last case, TNTHA was obtained by reacting the TNTs first with H, and then with A, using a molar ratio TNT:H:A = 1:1:1.

### Synthesis of PU and PU Nanocomposites Containing Modified TNTs

Pure PU and PU nanocomposites (modified TNTs) were synthesized according to the literature [8, 27], using a 500 mL glass reactor with five inputs, coupled to a mechanical stirrer, thermocouple (temperature control), reflux system, and an addition funnel. Pure PU was obtained by reacting PCL with H at a 1:1 molar ratio in 100 mL of MEK under inert atmosphere (N<sub>2</sub>), at 40°C for 2.5 h. DBTDL was used as the catalyst (0.1 wt% in relation to the total weight of reactants). In order to synthesize the nanocomposites, the fillers TNTH, TNTA, and TNTHA (1 wt% in relation to PCL weight) were previously suspended in MEK for 15 min under ultrasonification and the resulting suspensions were placed in the polymerization reactor. Nanocomposite films (~0.7 mm thick) were then prepared using the casting method.

## CHARACTERIZATIONS

TNTs and modified TNTs were characterized by Fourier transform infrared spectroscopy (FTIR, PerkinElmer spectrometer, Spectrum One model) using the accessory UATR (universal attenuated total reflectance), X-ray diffraction (XRD, Shimadzu XRD 7000, K $\alpha$  with  $\lambda$  = 1.542 Å, 40 kV, 30 mA, between 5° and 70° 2 $\theta$ , scanning speed of 0.02° min and counting time of 2.0 s), N<sub>2</sub> adsorption–desorption analysis (Micromeritics Instrument Corporation, TriStar II 302V1.03, recorded at 77 K in the 0.010 to 1.05 bar relative pressure range for 6 h) using the Brunauer–Emmett–Teller (BET) method, field emission scanning electron microscopy (FESEM, FEI Inspect F50 in secondary electron beam), and transmission electron microscopy (TEM, FEI Tecnai G2T20). The dimensions of TNTs were obtained by TEM analysis using Image J software (25 measurements).

The pure PU and PU nanocomposites containing modified TNT were characterized by analyzing the films via atomic force microscopy (AFM) to collect roughness data. The analyses were performed in tapping mode to construct phase/height contrast images at various locations on the sample surface, using a Bruker Dimension Icon PT system and TAP150A probe (Bruker, resonance frequency of 150 kHz and 5 N m<sup>-1</sup> spring constant). The equipment was calibrated prior to sample measurements. The scanned area of the images measured 2 × 2  $\mu$ m<sup>2</sup>, with a resolution of 512 frames per area. Dynamic mechanical analysis (DMA, model Q800, TA Instruments) with Young's modulus determinates according to ASTM D 882 standard technique. Both the TNTs and nanocomposites were submitted to thermogravimetric analysis (TGA, TA Instruments Q600, from room temperature to 1,000°C at a heating rate of 20 °C/min, under inert nitrogen). After solubilization in THF, the polymers were analyzed by gel permeation chromatography (GPC, Waters Instruments-2414), using a 1515 isocratic pump, tetrahydrofuran as mobile phase, flow rate of 1 mL/min and Waters 2414 refractive index detector,

with a Styragel column set (cut-off range: 500–500,000 g mol<sup>-1</sup>) at 45°C. Calibration curve was obtained with polystyrene standards.

The synthesized nanocomposites were also analyzed by differential scanning calorimetry (DSC, TA Instruments Q20, recorded from -90 to 200°C at a heating/cooling rate of 10 °C/min, under an inert N<sub>2</sub> atmosphere). The crystallinity ( $X_c$ ) of pure PU and its nanocomposites was calculated according to Eq. 1:

$$X_c = \frac{\Delta H_m}{(1-w)\Delta H_m^0} \quad (1)$$

where,  $\Delta H_m$  is the heat of fusion of the polymer or nanocomposite,  $\Delta H_m^0$  is the heat of fusion of 100% crystalline PCL (146 J g<sup>-1</sup>) [28] and  $w$  is the weight fraction of filler in the polymer matrix.

## RESULTS AND DISCUSSION

### Characterization of the Modified TNT

As shown in Fig. 1, TNTH are obtained via the reaction between the active hydrogen of the hydroxyl groups at the TNT surface and the isocyanate group ( $-N[\text{dbond}]C[\text{dbond}]O$ ) of the H molecule. On the other hand, interaction between the A molecule and OH groups of the TNT occurs via the methoxy group of the functionalizing agent [29], forming TNTA. Finally, TNTs modified using H and A molecules were obtained via the reaction between TNT and H, followed by interaction between the free NCO group of the H molecule anchored onto the TNT and the NH<sub>2</sub> group of the A molecule.

The SEM images of the modified TNTs and pristine TNT shown in Fig. 2 demonstrate that all the nanostructures are tubular and similar, corresponding to TNT agglomerates reported in the literature [20, 30]. In addition

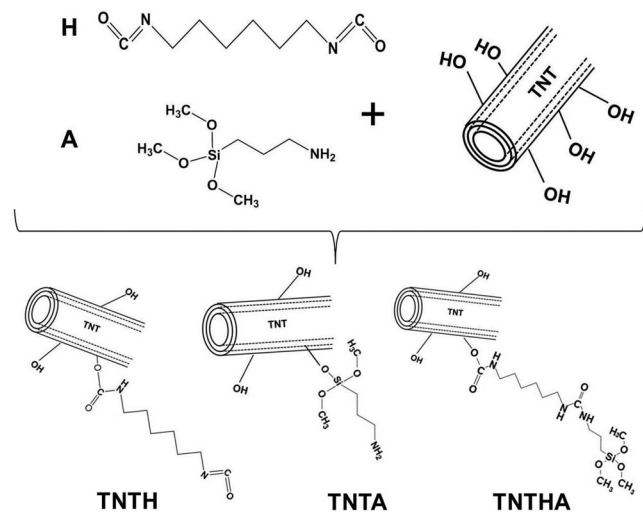


FIG. 1. Functionalization of the TNTs using H and A functional groups.

to detecting titanium and sodium corresponding to TNT, the results of Energy Dispersive X-ray Spectroscopy (EDS). analysis for each material (Fig. 2) indicate the presence of the functionalizing agents in the nanostructures, since carbon (from H and A molecules) and silicon atoms (from A molecules) were identified.

The TEM images of pristine TNTs and modified nanotubes (i.e., TNTH, TNTA, and TNTHA) shown in Fig. 3 indicate that the functionalization procedure did not affect the tubular structure of the TNT.

The pristine TNTs were formed by winding three titanate nanosheets together. Data on the average external and internal diameters of the TNTs, functionalized or not (Table 1), corroborate TEM images, that is, functionalization caused no significant changes.

For all the samples, the N<sub>2</sub> adsorption–desorption isotherms of the TNTs (Fig. 4) are type IV isotherm curves with a hysteresis cycle (H3) in the  $P/P_0 = 0.5-1$  interval. These isotherms indicate the presence of both mesopores (2–50 nm) and macropores (>50 nm) [31, 32].

Furthermore, the internal diameters recorded also corroborate the presence of mesopores, as shown and discussed above. A decrease in the pore volume (0.31, 0.42, and 0.19 cm<sup>3</sup>/g) and specific surface area values (56, 107, and 42 m<sup>2</sup>/g) of TNTH, TNTA, and TNTHA, respectively, was observed in relation to pristine TNT (0.55 cm<sup>3</sup>/g and 177 m<sup>2</sup>/g). This demonstrates that less N<sub>2</sub> is adsorbed onto the TNT surfaces, likely because the functionalization agents partially cover these surfaces. This result confirms that functionalization occurred through reactions of the OH groups located at the surface of the TNTs, behavior that is also reported in the literature [26].

Additionally, the isotherms in Fig. 4 demonstrate that the decline in  $S_{\text{BET}}$  values is associated with a decrease in hysteresis size in the following order: TNT > TNTA > TNTH > TNTHA. The same trend is observed for pore volume. This behavior also indicates that the presence of the functional group on the TNT lowers the number of pores, thereby reducing the amount of N<sub>2</sub> adsorbed during adsorption analysis.

Figure 5 shows the structural and chemical characterization of TNTs, TNTH, TNTA, and TNTHA obtained by FTIR and XRD analyses. With respect to pristine TNTs (Fig. 5a), the bands located between 3400 and 3300 cm<sup>-1</sup> and at 1640 cm<sup>-1</sup> correspond to the axial and angular deformation of the OH groups. Bands in the 900 and 750 cm<sup>-1</sup> region are assigned to the Ti—O stretching vibration of a four-coordinated Ti—O structure, and different vibration modes of Ti—O—Ti [15, 26, 33]. In relation to the FTIR spectra of TNTH (Fig. 5b), the band at 3360 cm<sup>-1</sup> corresponds to N—H stretching of urethane and the two bands in the 2930–2850 cm<sup>-1</sup> region to C—H stretching of the CH<sub>2</sub> group; bands at 1617 cm<sup>-1</sup> are assigned to C[dbond]O stretching, at 1575 cm<sup>-1</sup> to the C—N and N—H bonds of urethane and at 1255 cm<sup>-1</sup> to CO—O bonds [8, 34]. Given that the H agent has two NCO functions, the absence of a band at 2230 cm<sup>-1</sup> (free NCO)

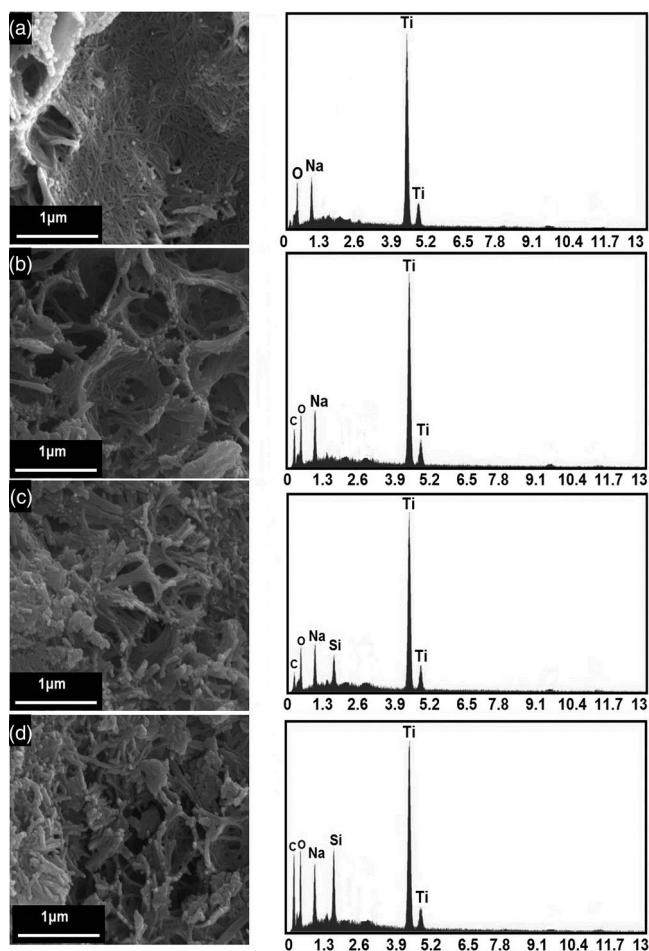


FIG. 2. SEM and EDS images of (a) pristine TNT, (b) TNTH, (c) TNTA, and (d) TNTHA (100k).

indicates that all the NCO groups reacted with the OH groups on the TNT surface. Likewise, the TNTA spectrum shows bands at  $2940\text{ cm}^{-1}$  (C—H of  $\text{CH}_2$  group),  $1330\text{ cm}^{-1}$  (C—N bond), and in the  $1120\text{--}1020\text{ cm}^{-1}$  region, corresponding to asymmetric stretching of the Si—O—Si bond [35], in addition to those characteristic of TNTs. The FTIR spectrum obtained for TNTHA exhibits characteristic bands of TNTs, HDI, and APTMS. It is interesting to note that, in addition to the bands corresponding

to TNTs, the spectrum also contains bands at  $3340\text{ cm}^{-1}$  (N—H stretching of urea and urethane linkages),  $2930\text{--}2850\text{ cm}^{-1}$  (C—H stretching of the  $\text{CH}_2$  group),  $1617\text{ cm}^{-1}$  (C[dbond]O stretching),  $1575\text{ cm}^{-1}$  (C—N and N—H bonds of urethane),  $1330\text{ cm}^{-1}$  (C—N bond),  $1255\text{ cm}^{-1}$  (CO—O bonds) and  $1130\text{--}1030\text{ cm}^{-1}$  (asymmetric stretching of the Si—O—Si bond) [8, 34, 36]. Modified TNT spectra displayed a band characteristic of the OH group, indicating that not all the OH groups of pristine TNT reacted during functionalization. With respect to the XRD pattern of pristine TNTs, the absence of a narrow peak at  $2\theta = 25^\circ$  (101), characteristic of  $\text{TiO}_2$  nanoparticles (attributed to the anatase phase), demonstrates complete transformation of  $\text{TiO}_2$  nanoparticles into TNTs. The XRD diffraction peaks at  $2\theta = 10^\circ$  (200),  $24^\circ$  (110),  $28^\circ$  (310),  $48^\circ$  (020), and  $62^\circ$  (422) are associated with lamellar titanates, whereas the peak at  $2\theta = 10^\circ$  is related to the interlayer distance [20, 26, 37, 38]. Interlayer distances for TNT, TNTH, TNTA, and TNTHA were 0.87, 0.90, 0.91, and 0.96 nm, respectively. This increase may be associated with the interaction of organic groups bonded to the surface of TNTs that replaced  $\text{Na}^+$  ions between the TNT layers, thus changing the original load balance and increasing the interlayer distance. Niu et al. also observed this behavior in TNT modified with amino groups used in heavy metal adsorption [39].

Figure 6 shows the thermogravimetric curves (TG and DTG) for pristine TNT and modified TNTs. Weight loss was observed in two steps for all the samples, namely in the  $25\text{--}100^\circ\text{C}$  and  $100\text{--}200^\circ\text{C}$  temperature ranges, associated with the decomposition of adsorbed water and the interlayer water, respectively. A decrease in the adsorbed and interlayer water content was observed for modified TNTs when compared to pristine TNTs (18%, 11%, 8%, and 10% for TNT, TNTH, TNTA, and TNTHA, respectively). These results indicate effective functionalization of TNT, since it promoted a decline in the number of OH groups present in pristine TNTs.

The degradation observed above  $200^\circ\text{C}$  corresponds to the organic segment used in functionalization. The results obtained were 13% for TNTH, 5% for TNTA, and 16.5% for TNTHA. Functionalization performed using the

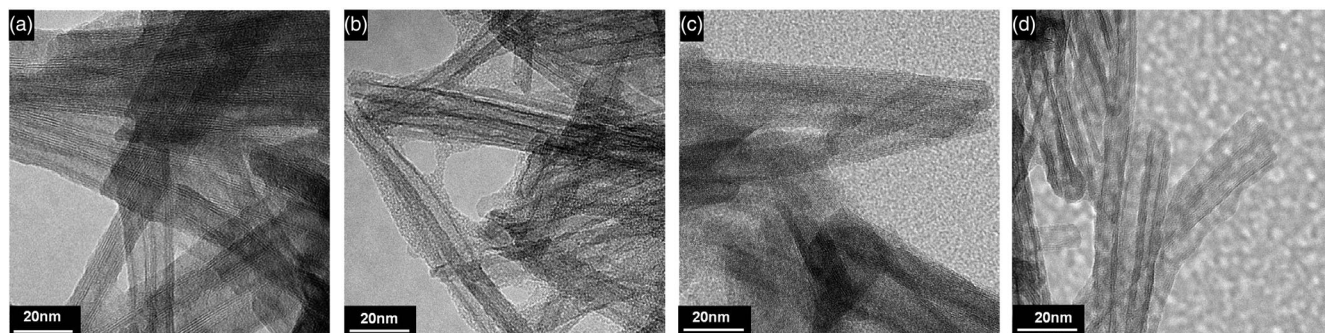


FIG. 3. TEM micrographs, magnification of 440k: (a) pristine TNT, (b) TNTH, (c) TNTA, and (d) TNTHA.

TABLE 1 Average diameters (external and internal) of the TNTs and their specific surface area ( $S_{BET}$ ).

Sample	Average external diameter (nm)	Average internal diameter (nm)	$S_{BET}$ (m <sup>2</sup> /g)	Pore volume (cm <sup>3</sup> /g)
TNT	9.8 ± 0.7	3.5 ± 0.4	177	0.55
TNTH	9.4 ± 2	3.5 ± 0.2	56	0.31
TNTA	10.6 ± 0.8	4.4 ± 0.5	107	0.42
TNTHA	8.6 ± 0.6	3.2 ± 0.3	42	0.19

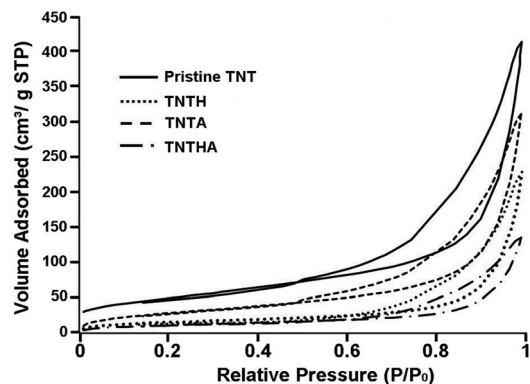


FIG. 4. N<sub>2</sub> adsorption-desorption isotherms of pristine TNT, TNTH, TNTA, and TNTHA.

diisocyanate molecule (TNTH and TNTHA) was more effective than that carried out with the amino reactant (A).

#### PU/Modified TNT Nanocomposite Characterization

The SEM, AFM, and TEM analyses were performed to assess PU matrix morphology and the degree of dispersion of the fillers. Figure 7a shows the spherulitic shape of the PU crystallites, which is characteristic of a polymer formed by chains containing soft (polyol) and hard segments (diisocyanate). The AFM image of this material shows dark and bright regions associated with amorphous (soft segments) and crystalline domains (hard segments),

respectively [40, 41]. Average roughness ( $R_a$ ) and root mean square roughness ( $R_q$ ) for pure PU and its nanocomposites were measured by AFM in tapping mode, obtaining  $R_a = 4.84$  nm and  $R_q = 6.25$  nm for pure PU. When 1 wt% of TNTH was added, the  $R_a$  and  $R_q$  values increased ( $R_a = 7.27$  nm and  $R_q = 9.25$  nm), indicating a rise in nanocomposite surface roughness with filler addition. This fact demonstrates that the TNTH filler influences the surface morphology of the polymer and leads to chain restructuring, whereby interaction with filler favors miscibility between polyol and diisocyanate (Fig. 7b). Previous research demonstrates that this filler reduces the ordering capacity of lamellae into three-dimensional spherulites, resulting in axialitic morphology [11]. This behavior was not observed for the TNTA filler, which showed the formation of different-sized spherulites. Figure 7c demonstrates that TNTA seems to have greater affinity with hard segments, probably due to hydrogen bonding between TNTA and the hard segments of PU. Verma et al. [42] observed the same behavior in modified cloisites. TNTHA addition resulted in a surprising morphology that was completely different from the others (Fig. 7d). A new organization occurred between the soft and hard domains, indicating that this filler interacted with both segment types. This is corroborated by the higher crystallinity degree observed in PU/TNTHA (34%) when compared to pure PU (27%), PU/TNTA (27%), and PU/TNTH (30%). The TNTA and TNTHA fillers prompted a decline in  $R_q$  and  $R_a$  when compared to pure PU, with  $R_a/R_q$  values of 4.32/5.45 nm and 4.48/5.79 nm for TNTA and TNTHA, respectively.

The dark regions in the TEM images indicate the presence of hard segments, since electron density is higher in these segments than in the soft segments. Figure 8b shows circular regions (hard segments) in the pure PU dispersed in a phase of soft segments, corroborating reports in the literature [5]. Images of the nanocomposites (Fig. 8c-h) show that fillers form small agglomerates that are well dispersed in the PU matrix.

FTIR analysis was also used to evaluate the interaction between the TNTs and PU chains (Fig. 9). The characteristic band at around 870 cm<sup>-1</sup> (Fig. 9a), corresponding to

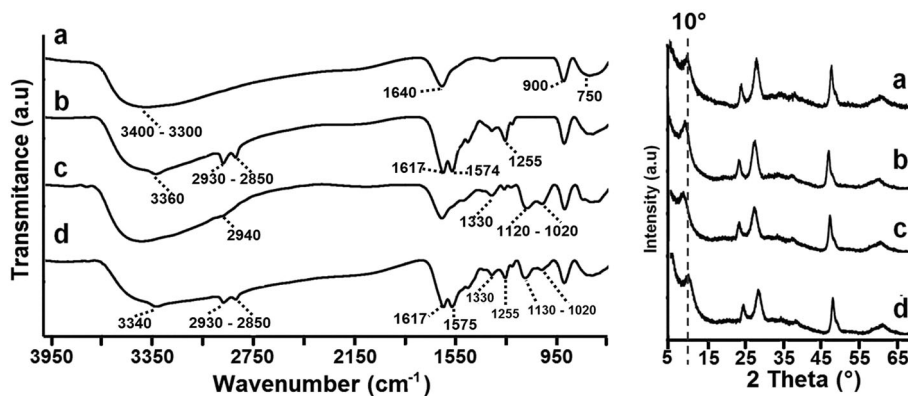


FIG. 5. Structural characterization of (a) pristine TNT, (b) TNTH, (c) TNTA, and (d) TNTHA by FTIR and XRD.

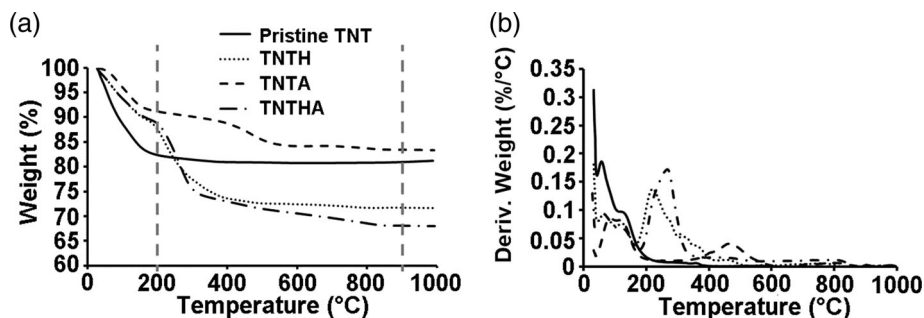


FIG. 6. TG (a) and DTG (b) curves of pristine TNT, TNTH, TNTA, and TNTHA.

Ti—O bond stretching [20], is very noticeable for PU/TNTH and PU/TNTHA and nonexistent for pure PU. A band at  $1160\text{ cm}^{-1}$  reflecting the C—O—C bond (Fig. 9b) exhibited differences when fillers were added: a shoulder is observed at  $1185\text{ cm}^{-1}$ , which may indicate interaction between the fillers and soft segments of the PU chains [6, 27, 43]. The urethane carbonyl stretching band at  $1680\text{--}1760\text{ cm}^{-1}$  was submitted to deconvolution and fitting to assess the influence of the fillers on the polymer matrix (Fig. 9c–f). The urethane carbonyl stretching band was then decomposed into three bands, namely a free carbonyl band at  $1734\text{ cm}^{-1}$ , a disordered hydrogen-bonded

carbonyl band at  $1703\text{ cm}^{-1}$ , and an ordered hydrogen-bonded carbonyl band at  $1683\text{ cm}^{-1}$  [44]. These three bands are only evident for pure PU (Fig. 9a). Addition of the fillers (Fig. 9d–f) prompted a significant increase and overlapping of the disordered and ordered hydrogen-bonded carbonyl bands, indicating a rise in the number of hydrogen bonds due to strong filler–polymer chain interactions.

The thermal and mechanical properties of the nanocomposites are shown in Table 2 and Fig. 10 presents the stress/strain curves. The onset temperatures obtained for the nanocomposites were at least  $10^\circ\text{C}$  higher than for pure PU, indicating that addition of the filler improved the thermal stability of the polymer. This is because the filler acts as a better thermal insulator and mass transport barrier, hindering heat and mass transfer [45, 46]. The  $T_g$  (soft segments) and  $T_m$  (hard segments) values of the nanocomposites remained unchanged in relation to pure PU. However, there was a significant increase in  $T_c$  among the nanocomposites, particularly for PU/TNTHA, demonstrating that the filler promoted better organization of the polymer chain.

The nanocomposite showed a reduction in molecular weights (Table 2), indicating competition between the surface OH groups of the functionalized filler and the OH groups of the PCL diol used in PU synthesis. The same behavior is reported in the literature [8, 9]. Comparison between pure PU and the nanocomposites revealed that, despite the decreased molar weight in the latter, a small decrease in Young's modulus was observed. However, stress at break values were similar and strain at break values higher than pure PU for the PU/TNTH. By contrast, these values were lower for nanocomposite TNTA, indicating that it is a more fragile material. This result can be explained by interaction between the filler and hard segments, thereby reducing PU chain mobility. The PU/TNTHA nanocomposite was the most promising, since the filler interacts with the hard and soft segments, providing greater crystallinity with different phase organization (Fig. 7d). This leads to increased elongation of the material without losing deformation resistance (Fig. 10), likely due to the greater mobility of the polymer chain resulting from the filler's compatibility with both segments.

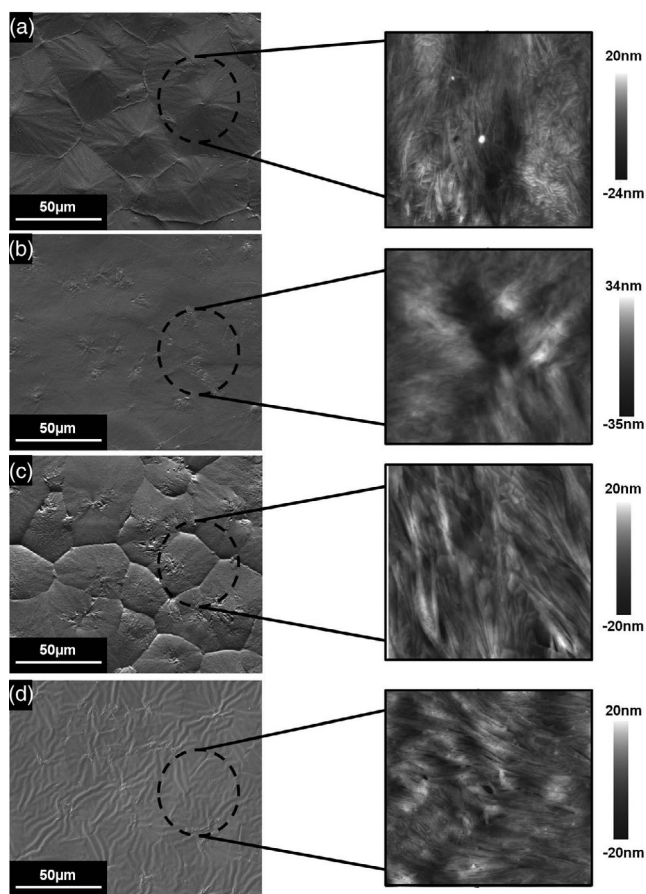


FIG. 7. SEM images (on the left), 2k magnification, and AFM images (to the right): (a) pure PU, (b) PU/TNTH, (c) PU/TNTA, and (d) PU/TNTHA.

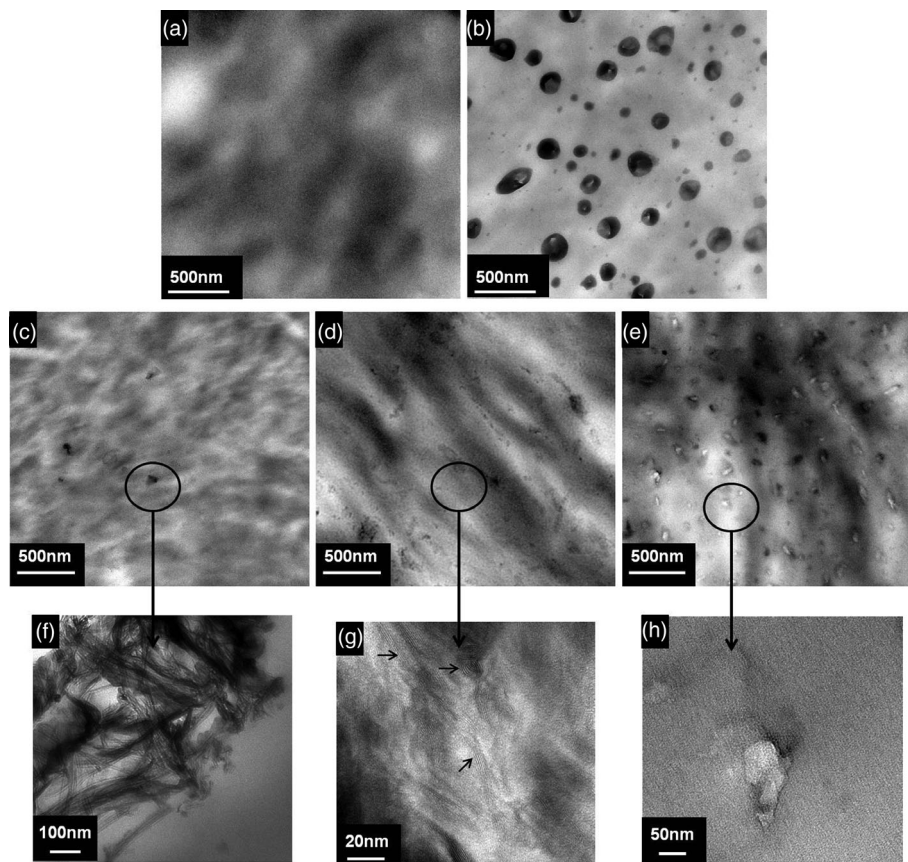


FIG. 8. TEM images of (a,b) pure PU, (c) PU/TNTH, (d) PU/TNTA, (e) PU/TNTHA at 140k magnification and (f) PU/TNTH, (g) PU/TNTA, and (h) PU/TNTHA at 410k magnification.

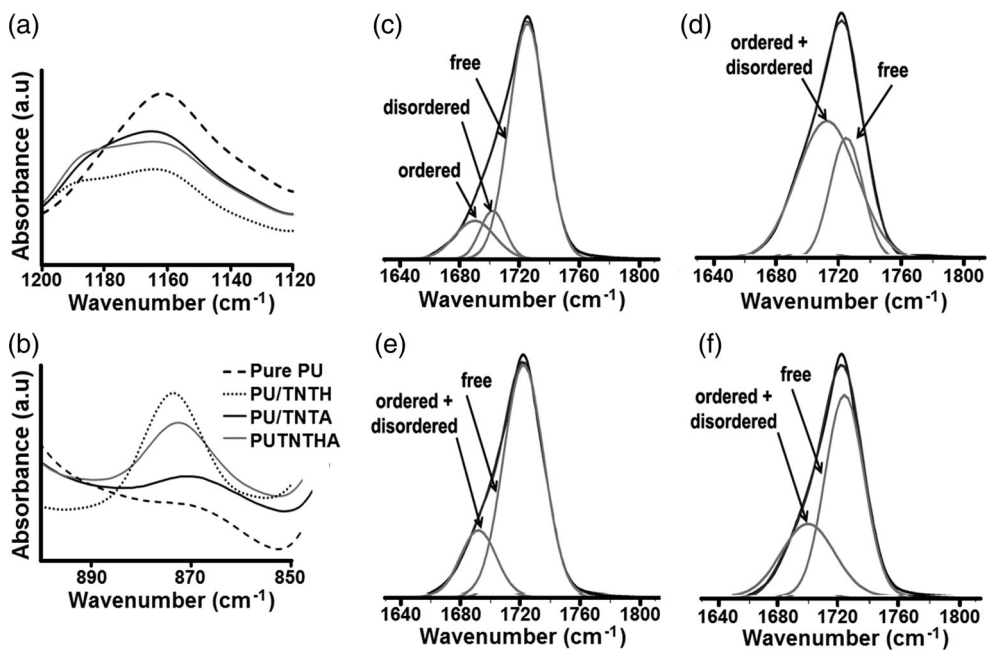


FIG. 9. Absorbance bands of pure PU and nanocomposites in the regions of (a)  $870\text{ cm}^{-1}$ , (b)  $1200\text{--}1160\text{ cm}^{-1}$  and deconvoluted curves of the carbonyl band of (c) pure PU, (d) PU/TNTH, (e) PU/TNTA, and (f) PU/TNTHA.

TABLE 2 Thermal, mechanical, and physicochemical properties of pure PU and nanocomposites.

Sample	$T_{\text{onset}}$ (°C)	$T_g$ (°C)	$T_c$ (°C)	$T_m$ (°C)	$M_w$ (g/mol)	$M_n$ (g/mol)	Stress at break (MPa)	Strain at break (%)	Young's modulus (MPa)
Pure PU	325 ± 1	-55	5.2 ± 0.1	43.9 ± 0.1	124,247	75,356	6.9 ± 0.7	4.5 ± 0.9	245 ± 37
PU/TNTH	335 ± 3	-55	6.5 ± 0.2	44.5 ± 0.1	113,046	65,237	6.0 ± 1.0	8.0 ± 0.9	160 ± 25
PU/TNTA	334 ± 2	-54	8.5 ± 0.1	44.6 ± 0.1	57,193	35,119	3.0 ± 1.0	2.0 ± 0.4	182 ± 22
PU/TNTHA	340 ± 2	-54	9.8 ± 0.1	44.9 ± 0.2	52,138	33,327	6.5 ± 0.4	22.0 ± 0.8	154 ± 22

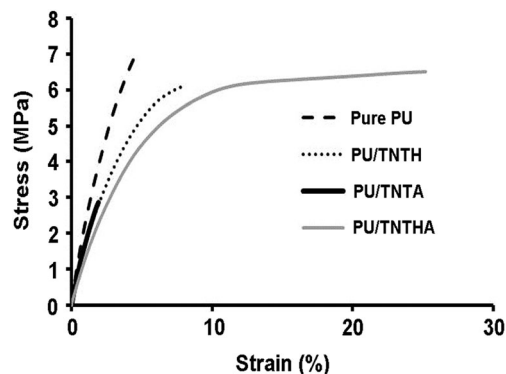


FIG. 10. Stress/strain curves for pure PU and PU nanocomposites.

The improvement in the mechanical properties of nanocomposite TNTHA, despite the low filler concentration and small surface area, may be associated with good filler dispersion due to greater filler–polymer than filler–filler interaction [9]. This corroborates the SEM, AFM, and TEM results and reinforces the idea that dispersion affects the mechanical properties of the nanocomposites.

## CONCLUSIONS

Aliphatic PU/modified TNT nanocomposites were prepared by *in situ* polymerization in order to obtain materials with superior thermal and mechanical properties. The functionalizing agents HDI (H) and APTMS (A) were used to obtain three different functionalized fillers, namely TNTH, TNTA, and a monourea segment (TNTHA). The amount of anchored organic segment was 5–16%. The hybrid nanotubes anchored with a monourea formed by HDI and APTMS (TNTHA) were found to be an interesting filler that significantly improved the mechanical and thermal properties of the PU nanocomposites.

## ACKNOWLEDGMENTS

The authors are grateful to PUCRS' Central Laboratory of Microscopy and Microanalysis (LabCEMM) for SEM, AFM, TEM, and EDS mapping.

Contract grant sponsor: CAPES (Coordination for the Improvement of Higher Education Personnel); Contract grant sponsor: CNPq (National Council for Scientific and Technological Development).

## REFERENCES

- D.L.P. Macuvele, J. Nones, J.V. Matsinhe, M.M. Lima, C. Soares, M.A. Fiori, and H.G. Riella, *Mater. Sci. Eng. C*, **76** 1248 (2017).
- J. Adhikari, B. Biswas, S. Chabri, N.R. Bandyopadhyay, P. Sawai, B.C. Mitra, and S. Arijit, *Eng. Sci. Technol. Int. J.*, **20**(2) 760 (2017).
- J. Bandyopadhyay, S.S. Ray, V. Ojijo, and M. Khoza, *Polymer*, **117** 37 (2017).
- W. Lei, C. Fang, X. Zhou, Y. Cheng, R. Yang, and D. Liu, *Thermochim. Acta*, **653** 116 (2017).
- S.K. Rath, V.K. Aswal, C. Sharma, and K. Joshi, *Polymer*, **55** 5198 (2014).
- R.B. Soares, W.F. Monteiro, C. Carone, S. Einloft, and R. Ligabue, *Polym. Bull.*, **71**(4) 829 (2014).
- X. Gao, Y. Zhu, X. Zhao, Z. Wang, D. An, and Y. Ma, *Appl. Surf. Sci.*, **257** 4719 (2011).
- V.D. Silva, L.M. Santos, S.M. Subda, R. Ligabue, M. Seferin, C.L.P. Carone, and S. Einloft, *Polym. Bull.*, **70**(6) 1819 (2013).
- M.A. Prado, G. Dias, C. Carone, R. Ligabue, A. Dumas, C. L. Roux, P. Micoud, F. Martin, and S. Einloft, *J. Appl. Polym. Sci.*, **132**(16) 1 (2015).
- L.M. Santos, R. Ligabue, A. Dumas, C.L. Roux, P. Micoud, J.F. Meunier, F. Martin, and S. Einloft, *Eur. Polym. J.*, **69** 38 (2015).
- M. Landa, J. Canales, M. Fernández, M.E. Munöz, and A. Santamaria, *Polym. Test.*, **35** 101 (2014).
- J. Marini, E. Pollet, L. Averous, and R.E.S. Bretas, *Polymer*, **55**(20) 5226 (2014).
- L. Jiang, C. Zhang, M. Liu, Z. Yang, W.W. Tjiu, and T. Liu, *Compos. Sci. Technol.*, **91** 98 (2014).
- T. Kasuga, M. Hiramatsu, A. Hoson, T. Sekino, and K. Niihara, *Langmuir*, **14** 3160 (1998).
- F. Yuan, C. Wu, Y. Cai, L. Zhang, J. Wang, L. Chen, X. Wang, S. Yang, and S. Wang, *Chem. Eng. J.*, **322** 353 (2017).
- J. Ma, F. Li, T. Qian, H. Liu, W. Liu, and D. Zhao, *Chem. Eng. J.*, **315** 191 (2017).
- L. Guo, J. Yang, G. Hu, X. Hu, H. DaCosta, and M. Fan, *Nano Energy*, **25** 1 (2016).
- G.R. Lima, W.F. Monteiro, R. Ligabue, and R.M.C. Santana, *Mater. Res.*, **20** 588 (2017).
- S.K. Parayil, A. Razzaq, S.M. Park, H.R. Kim, C.A. Grimes, and S.L. In, *Appl. Catal. A: Gen.*, **498** 205 (2015).

20. W.F. Monteiro, M.O. Vieira, A.S. Aquino, M.O. Souza, J. Lima, S. Einloft, and R. Ligabue, *Appl. Catal. A: Gen.*, **544** 46 (2017).
21. F. Sallem, R. Chassagnon, A. Megriche, M.E. Maaoui, and N. Millot, *J. Alloys Compd.*, **722** 785 (2017).
22. P.I. Pontón, J.R.M. Almeida, B.A. Marinkovic, S.M. Savic, L. Mancic, N.A. Rey, E.M. Junior, and F.C. Rizzo, *Appl. Surf. Sci.*, **301** 315 (2014).
23. Z. Shi, G. Xueping, S. Deying, Y. Zhou, and D. Yan, *Polymer*, **48**(26) 7516 (2007).
24. M.T. Byrne, J.E. McCarthy, M. Bent, R. Blake, Y. K. Gun'ko, E. Horvath, Z. Konya, A. Kukovecz, I. Kiricsi, and J.N. Coleman, *J. Mater. Chem.*, **17** 2351 (2007).
25. M. Sabzi, S.M. Mirabedini, J.Z. Mehr, and M. Atai, *Prog. Org. Coat.*, **65** 222 (2009).
26. L. Wang, W. Liu, T. Wang, and J. Ni, *Chem. Eng. J.*, **225** 153 (2013).
27. W.F. Monteiro, C.A.B. Santos, S. Einloft, M. Oberson, C.L. P. Carone, and R.A. Ligabue, *Macromol. Symp.*, **368** 93 (2016).
28. M.P. Arrieta and L. Peponi, *Eur. Polym. J.*, **89** 174 (2017).
29. H.J. Song, Z.Z. Zhang, and X.H. Men, *Eur. Polym. J.*, **44**(4) 1012 (2008).
30. J. Huang, Y. Cao, Z. Deng, and H. Tong, *J. Solid State Chem.*, **184**(3) 712 (2011).
31. R. Camposeco, S. Castillo, J. Navarrete, and R. Gomez, *Catal. Today*, **266** 90 (2016).
32. B. Erjavec, R. Kaplan, and A. Pintar, *Catal. Today*, **241** 15 (2015).
33. H.P. Chaos, C.K. Lee, L.C. Juang, and T.Y. Hsieh, *J. Taiwan Inst. Chem. Eng.*, **44**(1) 111 (2013).
34. D.L. Sun, J.Y. Luo, R.Y. Wen, J.R. Deng, and Z.S. Chao, *J. Hazard. Mater.*, **266** 167 (2014).
35. M.J. Palimi, M. Rostami, M. Mahdavian, and B. Ramezanzadeh, *Prog. Org. Coat.*, **77**(11) 1663 (2014).
36. Z. Ying, C. Zhang, S. Jiang, Q. Wu, B. Zhang, Y. Yu, M. Lan, H. Cheng, and F. Zhao, *J. CO2 Util.*, **15** 131 (2016).
37. J. Liu, Y. Liu, Z. Wu, X. Chen, H. Wang, and X. Weng, *J. Colloid Interface Sci.*, **386** 392 (2012).
38. D.C. Carvalho, A.C. Oliveira, O.P. Ferreira, J.M. Filho, S. T. Cuapa, and A.C. Oliveira, *Chem. Eng. J.*, **313** 1454 (2016).
39. G. Niu, W. Liu, T. Wang, and J. Ni, *J. Colloid Interface Sci.*, **401** 133 (2013).
40. A.S. Echart, L. Ugarte, C.G. Astrain, A. Arbelaiz, M. A. Corcuera, and A. Eceiza, *Carbohydr. Polym.*, **151** 1203 (2016).
41. I. Yilgör, E. Yilgör, and G.L. Wilkes, *Polymer*, **58** A1 (2015).
42. G. Verma, A. Kaushik, and A.K. Ghosh, *Prog. Org. Coat.*, **99** 282 (2016).
43. L. Bisticic, G. Baranovic, M. Leskovic, and E.G. Bajsic, *Eur. Polym. J.*, **46** 1975 (2010).
44. Y. Xu and D. Chen, *Mater. Chem. Phys.*, **195** 40 (2017).
45. H.D. Hwang and H.J. Kim, *React. Funct. Polym.*, **71**(6) 655 (2011).
46. T. Gurunathan and J.S. Chung, *Eng. Asp.*, **522** 124 (2017).